Carderock Division
Naval Surface Warfare Center
Bethesda, Md. 20084–5000

CARDIVNSWC–TR–61—94/25 August 1994
Survivability, Structures, and Materials Directorate
Technical Report

Experimental Application of Methodologies to Quantify the Effect of Constraint on J_c for a 3–D Flaw Geometry

by
W.C. Porr, Jr., R.E. Link and J.P. Waskey
Carderock Division, Naval Surface Warfare Center

and

R.H. Dodds, Jr.
University of Illinois

CARDIVNSWC–TR–61—94/25 Experimental Application of Methodologies to Quantify the Effect of Constraint on Jc for a 3–D Flaw Geometry

Carderock Division
Naval Surface Warfare Center
Bethesda, Md. 20084–5000

CARDIVNSWC–TR–61—94/25 August 1994
Survivability, Structures, and Materials Directorate
Technical Report

Experimental Application of Methodologies to Quantify the Effect of Constraint on J_c for a 3–D Flaw Geometry

by
W.C. Porr, Jr., R.E. Link and J.P. Waskey
Carderock Division, Naval Surface Warfare Center

and

R.H. Dodds, Jr.
University of Illinois

CONTENTS

FIGURES

TABLES

ABSTRACT

In an effort to validate methodologies to quantify the effect of crack tip constraint on cleavage fracture toughness, a series of experiments were conducted to measure the cleavage fracture toughness, J_c, of an ASTM A515 Grade 70 steel utilizing large plate bend specimens containing semi-elliptical surface cracks, SC(B), (3-D flaw geometry). J_c was estimated with modified EPRI and Turner design curve schemes from load and remote strains measured at initiation. The cleavage toughness of the A515 steel used for this testing was previously characterized using a series of through-cracked single edge notch bend specimens, SE(B), (2-D flaw geometry) with various initial crack-length to specimen-width ratios, a/W. The toughness values measured for the surface cracked plate specimens were consistent with the toughness ranges predicted from the SE(B) results using the toughness scaling and two parameter fracture mechanics (J-Q) methodologies to account for differences in crack tip constraint. This result verifies the applicability of small specimen, constraint adjusted, results to engineering structural integrity prediction for the case of cleavage fracture.

ADMINISTRATIVE INFORMATION

This work was performed at the Carderock Division, Naval Surface Warfare Center (CDNSWC), Annapolis Detachment, under the supervision of T. W. Montemarano, Head, Fatigue and Fracture Branch, as part of the program "Fracture Behavior of Naval Alloys Subjected to Explosive Loading Rates" (satisfies milestone 55FR3/10), under Work Unit No. 1-6140-503. Funding for this work was provided from the Office of Naval Research Ship and Submarine Materials Technology Program, Program Element No. 62234N, administered at CDNSWC by I. L. Caplan.

ACKNOWLEDGEMENTS

The authors would like to thank Dr. M. T. Kirk , formerly of CDNSWC, for contributing insight to this work through many helpful discussions, and providing the SE(B) data included in this manuscript.

INTRODUCTION

A fracture mechanics assessment of a structure is made by comparing the driving force for fracture with some measure of the materials resistance to

fracture. Traditionally, the fracture toughness of the material is expressed in terms of the critical value of a single parameter (eg. K, J, or CTOD). The fracture toughness is measured in the laboratory using small, deeply-cracked specimens with through cracks. This type of specimen is chosen because it has high constraint and is expected to yield a conservative measure of the toughness, provided certain size criteria are met. In calculating the driving force for fracture, it is frequently necessary to employ 2-D idealizations of the actual flaw in order to simplify the analysis and make use of existing tabulated crack solutions. This approach is generally thought to yield a conservative assessment of the fracture safety of a structure; however, there is no way of quantifying the degree of conservatism and such analyses may be overly conservative.

Driven by a desire to accurately establish the fracture integrity of flawed structures with laboratory scale testing, the fracture mechanics community has engaged in a considerable research effort to develop methodologies for quantifying the effect of crack tip constraint on unstable crack propagation behavior in pressure vessel steels (e.g. Refs. 1-9). The U.S. Navy has developed an interest in this work, not only for accurate structural integrity evaluation, but also to develop cost effective certification procedures for ship hull materials. Currently mandated explosive loading certification tests for hull steels are expensive and lack the quantitative results that allow interpretation to a variety of loading conditions and plate thicknesses. Development of a less expensive, laboratory scale material characterization procedure that will accurately and quantitatively predict the fracture behavior of explosively loaded steel hull structures may result in considerable cost and time savings to the U.S. Navy in ship hull material certification.

Two parameter fracture mechanics methodologies have been developed over the past several years which attempt to quantify material fracture toughness as a function of constraint [1-4]. The second parameter (Q or T) provides a quantitative measure of the level of constraint present in the structure or specimen. In these approaches, the material fracture toughness is not a single point value, but is described by a locus of toughness that varies with the applied constraint conditions. These approaches show the most promise for application in the ductile-brittle transition range of ferritic steels where the fracture toughness can be greatly influenced by the constraint conditions [3,5]. A related approach that has been developed along with the two-parameter methodologies is the toughness scaling model. The toughness scaling model incorporates a micromechanics-based failure criterion to determine the driving force which must be applied to a crack in a finite body in order to achieve a stressed volume equivalent to the critical stressed volume under small scale yielding conditions [6,7]. The various methodologies have been used to correlate experimentally observed effects of constraint on fracture toughness with some success [3-5,7].

All of the experimental validations of these two methodologies to quantify constraint reported to date have employed data from essentially 2-D, through cracked geometries. The critical test of these approaches will be the more

difficult problem of accurately predicting the response of structural elements containing realistic 3-D flaw geometries such as surface cracks. The surface crack introduces several difficulties that are not addressed by a 2-D approach to the problem. For 2-D analyses of through crack geometries, it is generally assumed that the crack tip conditions are uniform along the crack front. This is certainly not the case for the surface crack. For a given loading condition, the value of applied J varies considerably with position around the crack front [8]. The constraint also varies around the crack front, and the constraint variation may be completely different than that of J [9]. In the ductile-brittle transition region, there is also a size effect, related to the length of the crack front and associated with the probability of the incidence of a crack front cleavage initiation site, which is independent of the in-plane constraint effect [10]. No complete methodology has been developed yet which addresses all of these issues, and there are only very limited J and Q solutions for surface cracks currently available in the literature [8,9]. Nevertheless, experimental measurements of fracture behavior in specimens with surface cracks are needed in order to validate these new predictive models and guide their continued development.

This paper describes experiments conducted to verify the applicability of the toughness scaling and two parameter fracture mechanics methodologies to the surface crack geometry. The driving force, J, and Q were estimated based on available 2-D and 3-D results. The surface crack results were compared with conventional data developed from small laboratory specimens containing two dimensional flaws.

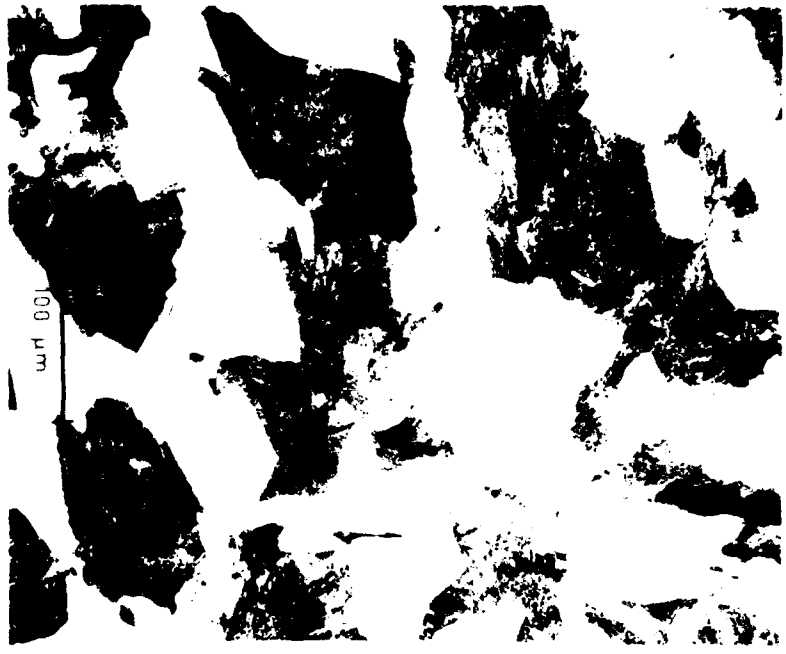

Figure 1--Mixed ferrite and pearlite microstructure of the ASTM A515 Grade 70 steel tested.

EXPERIMENTAL METHOD

Material

Specimen material used in this study is the same ASTM A515 grade 70 steel used in previous studies [3,4]. A515 is a C-Mn pressure vessel steel that is in transition at room temperature and shows significant plasticity before initiation of cleavage fracture. The microstructure of the material used in this study, illustrated in Figure 1, is mixed ferrite and pearlite, with an average grain diameter of approximately 75 micrometers.

The uniaxial tensile properties of the A515 are given in Table 1. For this study, Young's modulus, E, is assumed to be 207,000 MPa. The strain hardening coefficient given in Table 1 is defined by a fit to the stress-strain curve at stresses greater than the yield stress, σ_o, of the form:

$$\epsilon = \frac{\sigma_o}{E}\left(\frac{\sigma}{\sigma_o}\right)^n \qquad (1)$$

The lower the value of n, the greater the work hardening behavior of a material. A515, with a strain hardening coefficient of 4, is a high work hardening steel.

TABLE 1--Tensile properties of ASTM A515 Grade 70 steel at 20° C

0.2% Yield strength, MPa	Tensile strength, MPa	Flow strength, MPa	% Elongation, in 25.4 mm	% Reduction in area	Strain hardening coefficient
288	542	415	34	51	4

Specimen Geometry

The large plate, surface cracked bend, SC(B), specimen tested in this study is illustrated in Figure 2. Plate dimensions were 50.8 mm in thickness, 203.2 mm in width, and 584.2 mm in length. This approximates a geometry used by the U.S. Navy for hull material characterization under explosive loading. Cracks were oriented in the T-S direction relative to plate processing. Semi-elliptical surface cracks were grown by fatigue from electric discharge machining (EDM) slots in the center of the specimens.

Three different nominal crack geometries were tested in this study. The three different geometries are indicated in Figure 2 and Table 2, with actual crack dimensions for all successfully tested specimens given in Table 3. Crack geometry 1 (a = 6.35 mm and 2c = 17.8 mm), was utilized for only two specimens, GGR2-1

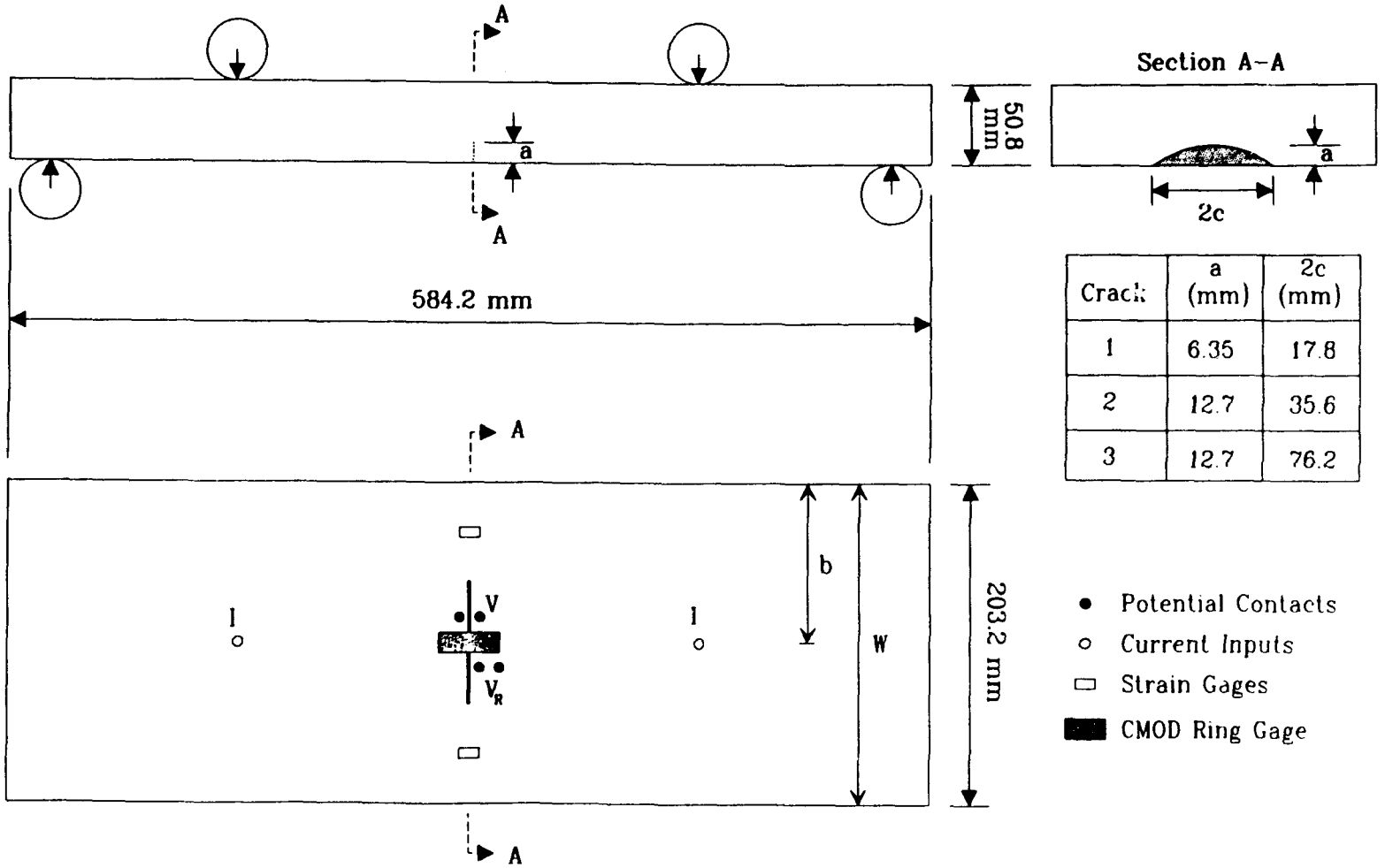

Figure 2 Large plate, surface cracked bend, SC(B), specimen geometry tested in the current study.

and GGR2-2. Neither test yielded data that could be analyzed in this study, and will only be further discussed briefly in the RESULTS section, below.

TABLE 2--Nominal crack dimensions for the SC(B) specimens tested

Geometry	2c/a	a/t	a (mm)	2c (mm)
1	2.8	0.125	6.35	17.8
2	2.8	0.25	12.7	35.6
3	6.0	0.25	12.7	76.2

Fatigue precracking was performed in three-point bending at a constant load amplitude. The cyclic moment range was approximately 17.2 kN-m, and the stress (moment) ratio, R, was approximately 0.2. This loading resulted in maximum ΔK's of approximately 12.6 MPa$\sqrt{m}$ for crack geometry 2 and 14.8 MPa$\sqrt{m}$ for crack geometry 3, at the end of precracking. Initial EDM slot dimensions were selected to result in specific crack geometries following precracking. Using stress intensity (K) solutions for semi-elliptical surface cracks in plates subjected to bending loads [11] and assuming steady state fatigue crack growth ($da/dN = C\Delta K^m$), EDM slot dimensions required could be inferred from desired final crack dimensions. Stress intensity varies around the semi-elliptical crack front for a given remote load:

$$K = S_b\sqrt{\pi a} \cdot f\left(\frac{a}{c}, \frac{a}{t}, \frac{c}{b}, \Phi\right) \qquad (2)$$

where S is the bending moment, a is the crack depth, c is the half surface length, t is the plate thickness, b is the plate half-width, and Φ is the parametric angle of ellipse. K is typically higher at the maximum depth than at the surface for the cracks examined here. The semi-elliptical crack grew at different rates in the depth and along the plate surface, hence, initial depth (a) to surface length (2c) aspect ratio (2c/a) was not necessarily the same as the desired final aspect ratio. Additionally, EDM slot depth was reduced from that dictated by this method to account for crack initiation at the maximum depth (higher initial ΔK) prior to initiation on the surface.

Testing Procedure

SC(B) specimens were loaded in four point bending under a constant crosshead displacement rate of 2.12×10^{-5} m/s (Figure 3). The moment arm for

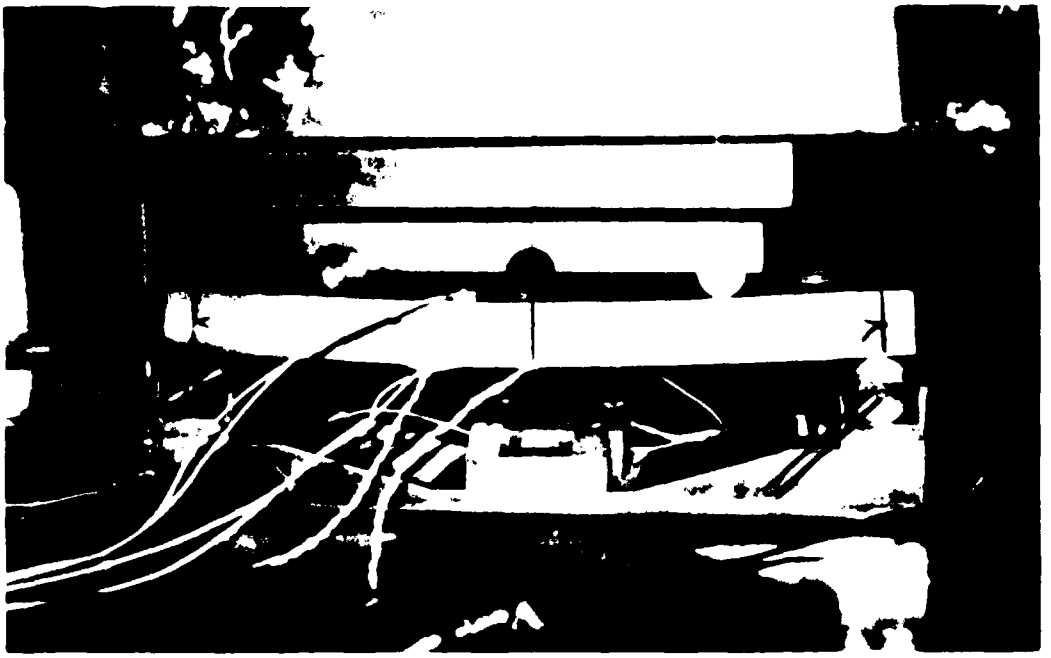

Figure 3--Large plate, SC(B) specimen loaded in four point bending.

applied loading was 121 mm. Load, crack mouth opening displacement (CMOD), remote strain, and AC potential difference (ACPD) across the crack mouth were monitored continuously during loading. CMOD was measured by a ring gage inserted at the crack mouth on the center line of the specimen. Remote strain was measured at ±0.5 b on the crack plane, on both the front and back faces of the plate. The parameter b is defined as the distance from the centerline to the plate edge in the plate width. ACPD was measured to indicate any ductile crack extension prior to the initiation of cleavage fracture. Neither the ACPD data nor the CMOD data were necessary for the analyses conducted in his study, but will be used for additional analyses to be conducted in the future.

J Integral Estimation

J integral values at cleavage initiation, J_c, were determined using two approximations that had previously been shown to be effective in estimating J for the SC(B) specimen geometries 2 and 3 with a different material response [8].

For crack geometry 2, an engineering-J design curve formulation [12] was used to estimate J_c from remote strains. The design curve formulation was developed from two-dimensional elastic-plastic plane-strain finite-element analyses of a variety of cracked body geometries and loading conditions, for cracks with $a/W \leq 0.1$ [12]. When yielding has occurred in the 'gross section' of the specimen

(i.e. $e/e_y > 1.2$), the engineering-J design curve methodology provides that J can be estimated by:

$$J = 2.5\left[\left(\frac{e}{e_y}\right) - 0.2\right]G_y \tag{3}$$

where e is remote strain for the uncracked body, e_y is the yield strain (σ_o/E), and $G_y = K^2_{Iy}/E$. K_{Iy} is given by solving equation 2 with $S_b = S_c$, the bending moment for outer fiber yielding.

For crack geometry 3, a modified EPRI estimation scheme [13] was used. The EPRI methodology for determining J was developed from consideration of cracks in stressed bodies where material flow behavior is described by:

$$\frac{\epsilon}{\epsilon_o} = \frac{\sigma}{\sigma_o} + \alpha\left(\frac{\sigma}{\sigma_o}\right)^n \tag{4}$$

where α is a constant (≈ 1) and $\epsilon_o = \sigma_o/E$. J is given by:

$$J = J_e + J_p \tag{5}$$

where J_e is defined as:

$$J_e = \frac{K^2(a_{eff})}{E'} \tag{6}$$

where E' is E for plane stress and $E/(1-\upsilon^2)$ for plane strain, υ is Poisson's ratio, and $K(a_{eff})$ is the stress intensity for the given plastic zone corrected crack length and applied loading. Plastic zone corrected crack length, a_{eff}, is given by:

$$a_{eff} = a + \frac{1}{\beta\pi}\left(\frac{n-1}{n+1}\right)\left(\frac{K}{\sigma_o}\right)^2 \frac{1}{1+\left(\frac{P}{P_L}\right)^2} \tag{7}$$

where β is 2 for plane stress and 6 for plane strain, P is applied load, and P_L is the specimen plastic limit load. Limit load was estimated for each specimen by determining an equivalent through edge crack depth, a_{eq} for the surface crack in the plate geometry [14],

$$a_{eq} = \frac{\pi a c}{4c + 2t} \tag{8}$$

and solving for limit load of this through edge crack:

$$P_L = \frac{\sigma_o B (t - a_{eq})^2}{4L} \tag{9}$$

where B is plate width (=2b) and L is the moment arm length. Modification of the EPRI methodology, incorporating a reference stress ($\sigma_o \bullet P/P_L$) and the assumption that a non-dimensional geometry factor is independent of work hardening [13], results in J_p approximated as:

$$J_p = \frac{\mu K^2(a)}{E}\left[\left(\frac{P}{P_L}\right)^{n-1} - 1\right] \tag{10}$$

where μ is 1 for plane stress and 0.75 for plane strain.[1]

RESULTS

J Integral Estimation

It was determined early in the test program that crack geometry 1, with a ≈ 6.4 mm and 2c ≈ 17.8, would not yield the desired cleavage fracture data at the test temperature, 20°C. Extensive ductile crack extension occurred in the two specimens of this crack geometry tested, GGR2-1 and GGR2-2, without subsequent initiation of cleavage fracture. This geometry was then abandoned for crack geometry 2, with a ≈ 12.7 mm and 2c ≈ 35.6 mm. Crack geometry 2 has approximately the same crack aspect ratio of 2c/a = 2.8 as geometry 1, but is four times larger by area. The load and strain at the initiation of cleavage fracture, P_c and e_c, from the seven successful experiments with specimen geometry 2 and ten experiments with geometry 3 are given in Table 3. One specimen with crack geometry 2 (GGR2-10) did not fail before the displacement (≈50 mm, center-line) and load limits (≈1300 kN) of the test fixtures and load frame were reached.

---

[1] Equation 9 varies from that reported in Ref. 13 with $\sigma_o/E \bullet (\sigma_{ref}/\sigma_o)^n$ substituted for ϵ_{ref}, where $\sigma_{ref} = (P/P_L)\sigma_o$.

TABLE 3--Test specimen data

Specimen ID	a_i (mm)	$2c_i$ (mm)	$2c/a_i$	a/t_i	Δa (mm)	a_f (mm)	$2c_f$ (mm)	P_L (kN)	P_o (kN)	e_o	J_o (kJ/m^2)
GGR2-3	11.2	32.5	2.89	0.221	2.36	13.6	35.1	273.6	626.1	0.0498[1]	391.2
GGR2-4	13.3	37.7	2.84	0.261	0.13	13.4	37.7	262.0	419.0	0.0180	154.3
GGR2-5	10.5	31.9	3.03	0.207	1.60	12.1	33.9	276.2	572.5	0.0398[1]	337.0
GGR2-6	11.9	35.2	2.96	0.234	0.00	11.9	35.2	269.1	446.4	0.0218[1]	193.3
GGR2-7	12.2	35.3	2.89	0.240	0.00	12.2	35.3	267.8	453.0	0.0229	105.3[2]
GGR2-8	12.9	38.7	3.00	0.254	0.00	12.9	38.7	262.4	379.6	0.0171	97.5[2]
GGR2-9	13.6	37.1	2.72	0.268	0.00	13.6	37.1	261.2	421.4	0.0180	149.0
GGR6-1	12.2	77.5	6.36	0.240	0.00	12.2	77.5	246.9	338.9	0.0085	55.4
GGR6-2	11.4	78.3	6.88	0.224	0.00	11.4	78.3	250.9	342.7	0.0110[1]	56.4
GGR6-3	10.9	80.3	7.33	0.216	0.38	11.3	80.3	252.6	388.8	0.0193	104.2
GGR6-4	12.8	79.4	6.19	0.253	1.14	13.9	79.4	243.3	453.3	0.0269[1]	242.1
GGR6-5	12.1	76.6	6.34	0.238	0.28	12.4	76.6	247.8	372.7	0.0137	86.9
GGR6-6	12.7	76.4	6.02	0.250	0.64	13.3	76.4	244.6	409.0	0.0197	140.8
GGR6-7	13.4	77.8	5.8	0.264	0.00	13.4	77.8	240.6	330.3	0.0093	51.9
GGR6-8	12.4	77.4	6.22	0.245	0.00	12.4	77.4	245.5	340.3	0.0092	57.3[2]
GGR6-9	13.7	81.5	5.94	0.270	0.00	13.7	81.5	237.5	374.7	0.0131	103.6
GGR6-10	14.5	79.5	5.49	0.285	0.00	14.5	79.5	234.4	335.6	0.0102	60.2

[1] Extrapolated
[2] Pop-in

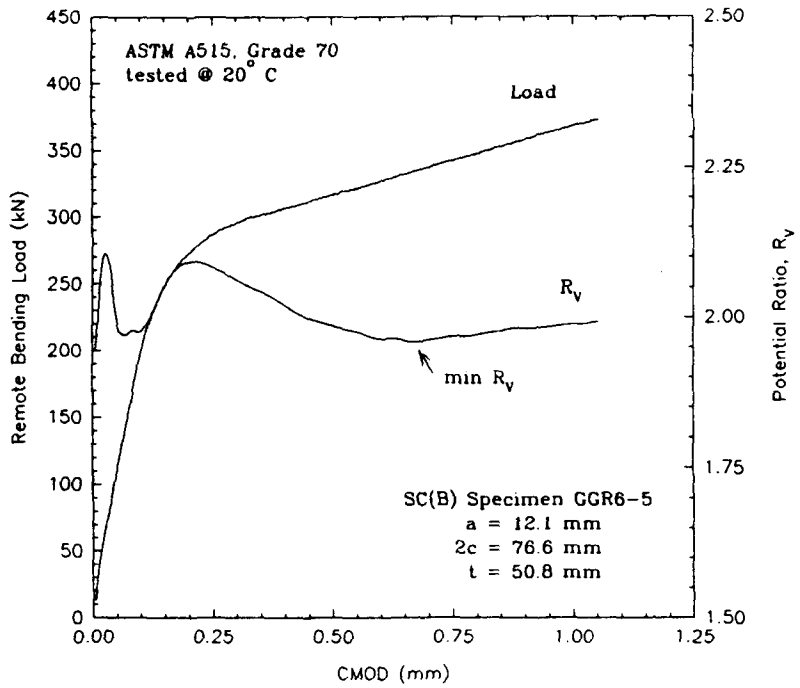

(a)

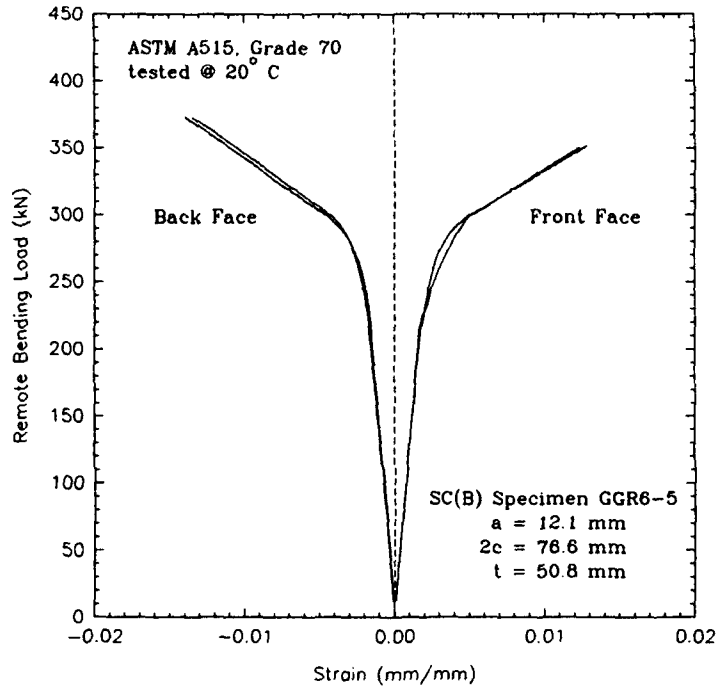

(b)

Figure 4--(a) Load and potential ratio versus crack mouth opening displacement (CMOD), and (b) load versus remote strain, for SC(B) specimen GGR6-5.

An example of recorded data is given in Figures 4a and 4b. Applied bending load (½ of load cell output) and ACPD potential ratio, R_V, are plotted versus CMOD for specimen GGR6-5 in Figure 4a. The potential ratio, R_V is defined as V/V_r, where V is the potential across the crack mouth and V_r is the reference potential. Bending load is plotted versus monitored remote strains for the same specimen in Figure 4b. The monitored data was relatively free of noise, with the exception of the ACPD data which is shown after smoothing. The strain at cleavage fracture had to be extrapolated from lower strains in several cases after strain gages debonded from the specimen during loading. In three instances cleavage initiation was indicated by crack "pop-in", where a burst of cleavage cracking occurred without causing total separation of the plate specimen. Total specimen failure then occurred with additional loading.

Following specimen failure, fracture surface examination at low magnification confirmed the cleavage fracture mode and allowed accurate precrack measurement (Figure 5). As indicated in Table 3, six of the specimens with crack geometry 3 and four specimens with geometry 2 failed by cleavage with no prior ductile crack extension. The other specimens exhibited varying amounts of crack extension less than 2 mm, with the exception of specimen GGR2-3. Crack extension was measured at the maximum depth. ACPD was successful at indicating the occurrence of ductile crack extension during loading, but unsuccessful in correctly measuring the amount of extension without post-test analysis. For the purposes of the current study, a real time measure of crack

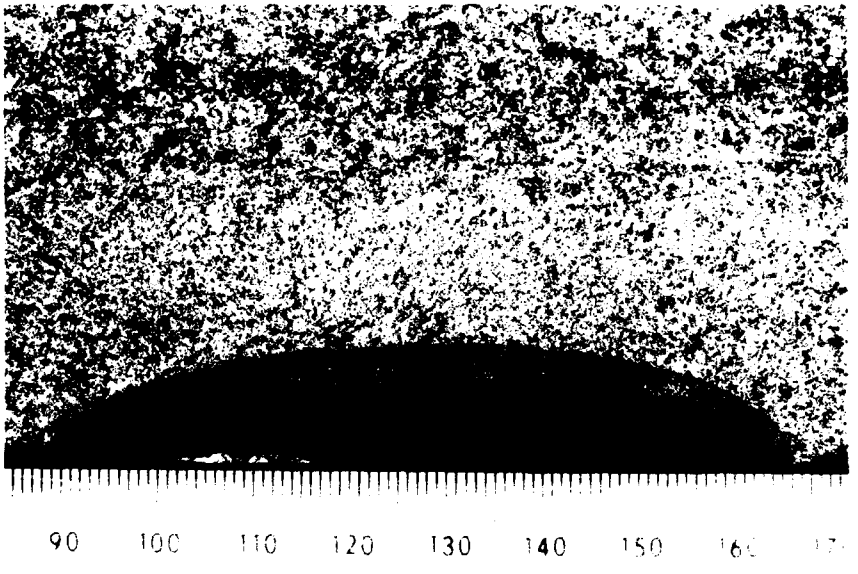

Figure 5--Low magnification image of the semi-elliptical 2c/a = 6 flaw for SC(B) specimen GGR6-8. Scale shown is in units of millimeters (mm).

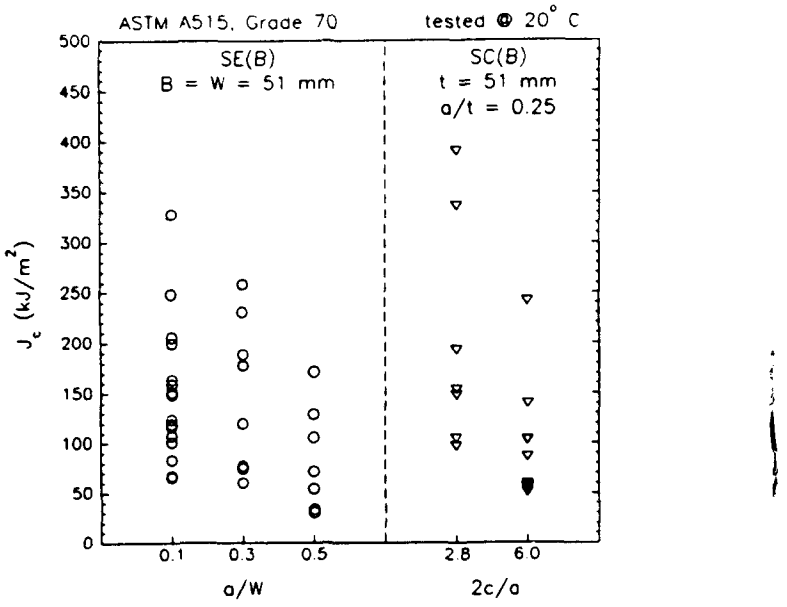

Figure 6--Cleavage toughness (J_c) values for A515, Gr. 70 steel measured using SE(B) [3] and SC(B) specimens with nominal geometries shown.

extension was not critical. ACPD was used primarily as a condition monitoring tool in this study with future analysis of the data to characterize the effect of ductile tearing on cleavage initiation possible.

J_c values for the tested specimens were estimated using the techniques described above with the results indicated in Figure 6 and Table 3. Values shown for geometry 3 are the average of the plane strain and plane stress values determined with the EPRI estimation. Figure 6 plots the measured cleavage toughness as a function of specimen geometry. Results for the A515 cleavage fracture toughness determined using SE(B) specimens with crack depth ranging from a/W = 0.1 to a/W = 0.55 [3] are also plotted in Figure 6 for comparison. Toughness values ranged from 51.9 kJ/m^2 to 242.1 kJ/m^2 for crack geometry 3, and from 97.5 kJ/m^2 to 337.0 kJ/m^2 for crack geometry 2. The range of measured toughness values for geometry 3 approximates the range for SE(B) specimens with a/W≈0.3, while that associated with geometry 2 approximates the cleavage toughness range for SE(B) specimens with a/W≈0.1.

Multi-specimen fracture resistance curves developed from the SE(B) data of Kirk et al. [3] and the SC(B) data for crack geometry 3 from this study are presented in Figure 7. J values at cleavage were plotted versus the amount of ductile crack extension prior to cleavage initiation. The R-curve produced this way includes crack tip blunting with the measured crack extension. From these plots, an approximate initiation J, J_i, for ductile crack extension can be determined by the intersection with the blunting line ($J=2\sigma_{flow}\bullet\Delta a$) of a regression

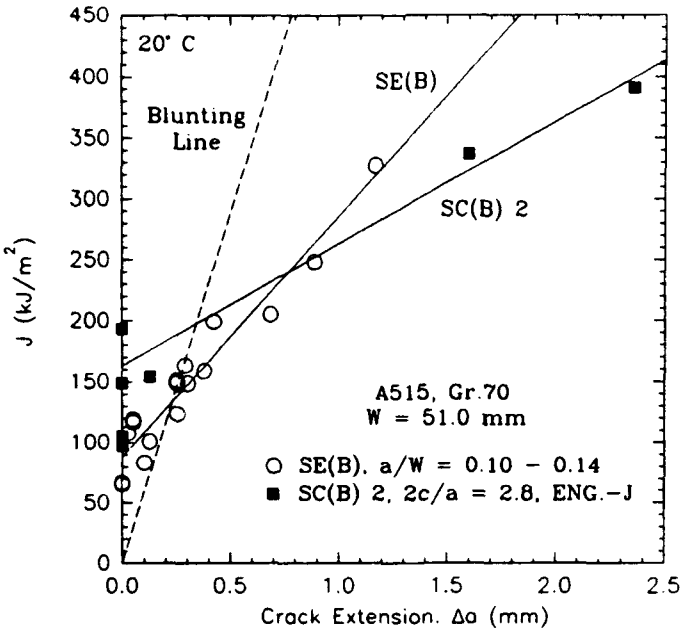

(a)

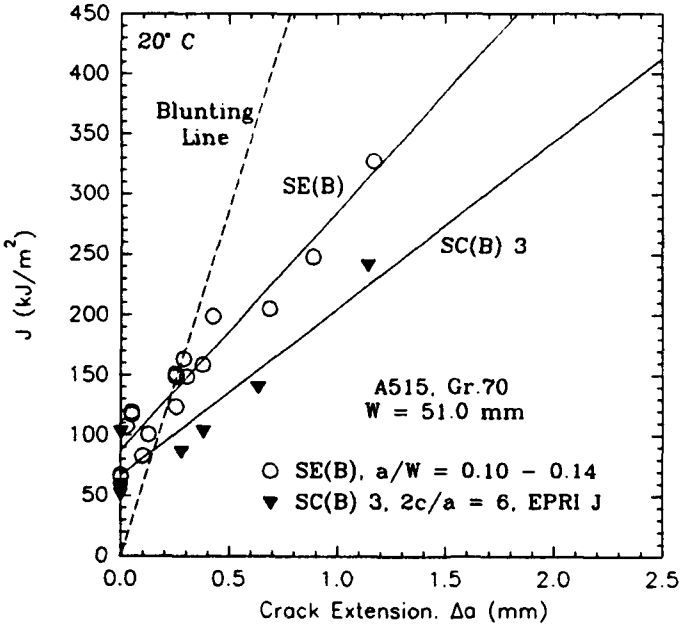

(b)

Figure 7--Multi-specimen R-curves for A515, Gr. 70 steel determined with SC(B) specimens for (a) 2c/a = 2.8 with J determined from engineering J design curve, and (b) 2c/a = 6 with J determined from modified EPRI formulation. Data from SE(B) specimens with a/W = 0.1 [3] plotted for comparison.

line drawn through the data. J_{IC} for ductile crack extension has been previously shown to be relatively insensitive to specimen geometry for a given material [15]. Therefore, comparison of the J_i for each of the data sets should give an indication of the accuracy of the estimation schemes used for SC(B) J analysis. As indicated in Figure 7, J_i for ductile crack extension in the A515 steel is approximately 135 kJ/m^2 according to the SE(B) data of Kirk et al. [3]. The J_i indicated by the regression through the SC(B) data for crack geometry 3 from this study is approximately 89 kJ/m^2. This implies that the estimation scheme used to determine applied J for the SC(B) specimen with crack geometry 3 underestimates the true J-integral at the crack front. This result is consistant with a previous analysis of the anticipated effectiveness of the EPRI estimation for an SC(B) specimen at strains well beyond yield [8]. Similarly, the J_i for the SC(B) specimen with crack geometry 2 is approximately 197 kJ/m^2, indicating that the engineering-J design curve overestimates the true applied J-integral in this case.[2]

Application of Constraint Methodologies

Experimental application of constraint methodologies to the data developed in the current study can only be accomplished by making numerous estimations. Future work will include the finite element modelling to develop the necessary J integral and constraint solutions for this material and specimen geometry. Finite element modelling has been performed for surface cracked tension, SC(T), specimens of the lower hardening, higher strength, pressure vessel steel ASTM A533B [9], and for SC(B) specimens with different flow properties than the material examined in the current study [8]. Results of that modelling are used here to estimate the applicable Q values for the SC(B) A515 data.

For the J values determined for crack geometry 3 using the modified EPRI estimation scheme described previously, Q values were estimated graphically from the uniaxial tension J-Q driving force curves in Dodds et al. [9] and then adjusted to higher constraint values to account for the higher hardening material and bend loading. The amount of the adjustment ($\approx +0.25$) to Q was selected based on previously reported dependence of Q on strain hardening coefficent for the SE(B) geometry [3,9]. The value of Q for a given J_c for crack geometry 2 was estimated as approximately equal to that for the larger surface flaw in the lower hardening material. Prior modelling of this type of flaw [8,9] indicates that the highest J and

---

[2] Two different estimation schemes were used to determine J_c for the two SC(B) geometries; if the same estimation technique was used for all of the data, it was found that the engineering-J design curve formulation apparently overestimated the true J at the crack tip for geometry 3 as well. Likewise, the EPRI estimation apparently underestimated the true crack-tip J for geometry 2. A determination as to which technique is more appropriate to use for the SC(B) specimens of this material is not made here.

crack tip constraint for a surface crack is not necessarily at the maximum depth. For the purposes of this study however, initiation is assumed at the maximum depth. The maximum J given by the two J estimation schemes used is at the maximum depth.

Figure 8 shows the application of the two parameter fracture mechanics (J-Q) methodology to assess the effect of constraint on the cleavage fracture toughness. Plotted are the A515 data for the SC(B) specimens of this study and the SE(B) data of Kirk et al. [3] (with a crack growth restriction as indicated). If the J-Q driving force curve for crack geometry 3 is estimated as described above and shown in Figure 8, then SC(B) measured cleavage toughness values should fall along the curve, within the J-Q toughness locus developed from SE(B) specimens with various a/W. Examination of the values estimated indicates that the data for crack geometry 3 are within the range of the SE(B) J-Q locus. Even if the actual J_c values for this geometry are approximately 50% higher than the estimates, as implied by the data in Figure 7, then the data for the SC(B) geometries would still fall within the J-Q locus. The implication from these results is that the cleavage fracture integrity of a structure can be determined using computer modelling to determine the applicable J-Q driving curve, and the J-Q locus for the material developed from standard fracture specimen laboratory tests coupled with the constraint indexing methodology.

Application of the toughness scaling methodology to the SC(B) data is not as straightforward. The general approach to validate any modelling would be to

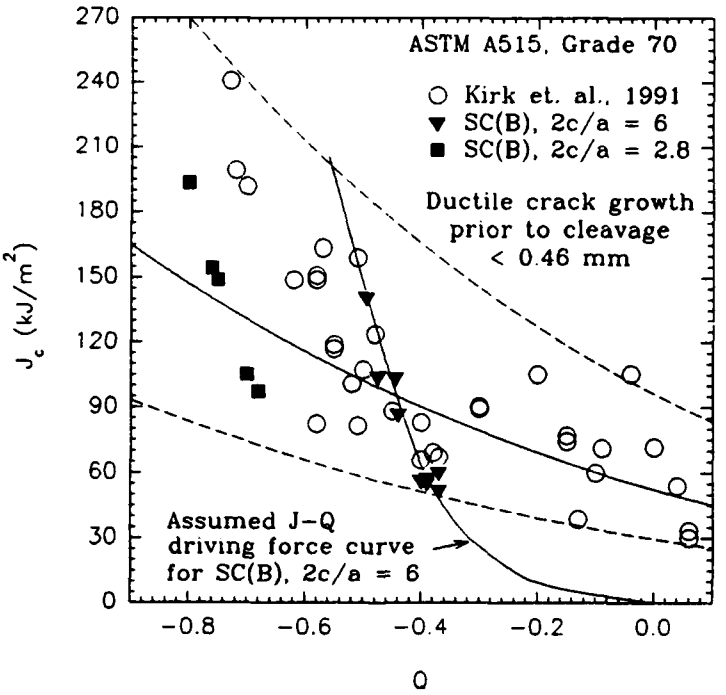

Figure 8--Application of two parameter fracture mechanics methodology. J-Q fracture toughness locus developed from SE(B) data [3].

determine the range of J_o for the A515 from constraint corrected SE(B) data, and then determine the range of predicted J_c for the the two SC(B) geometries from toughness scaling driving force curves for cleavage fracture. Measured data would then be compared to these ranges. At this time, however, the finite element modelling to develop the driving force curves for the A515 SC(B) specimens has not been completed.

Another approach to utilize the toughness scaling approach to quantify constraint effects in cleavage fracture is possible. The toughness scaling driving force curves for the two SC(B) geometries studied could be matched to approximately equivalent driving force curves of SE(B) specimens [9]. If it were assumed that the J values determined for the experiments of this study were accurate, the implication of the data in Figure 6 is that the toughness scaling driving force curve for an SE(B) specimen with a/W of $\approx$ 0.1 could be used to approximate the response of SC(B) specimen geometry 2. Likewise, the driving force curve for the SE(B) specimen with a/W $\approx$ 0.3 could be used to approximate the response of SC(B) specimen geometry 3.

Future Work

Finite element modelling (3-D) will be conducted to determine the appropriate J and Q values, and toughness scaling driving force curves as a function of the material behavior, loading parameters, and position along the crack front for the two SC(B) geometries tested in this study. This will be coupled with measurements of the angle of cleavage initiation site along the crack front of each of the SC(B) specimens, determined from detailed scanning electron microscopy (SEM). In that way, accurate application of the two methodologies to quantify the effect of constraint on cleavage fracture initiation can be conducted to demonstrate that data from small laboratory specimens with 2-D flaws can be used to predict the fracture integrity of a structure containing a 3-D flaw. Preliminary SEM has indicated cleavage initiation site angles of approximately 44° and 37° for specimens GGR6-1 and GGR6-2 respectively.

CONCLUSIONS

The following conclusions can be made from the data and analyses presented:

1. Multi-specimen fracture resistance curves for the A515 steel used in this study, developed from SC(B) and SE(B) data, indicated that J_c values estimated for SC(B) specimen geometry 3 were lower than actual J_c values, and those estimated for SC(B) geometry 2 were higher. J_c values estimated are sufficiently accurate for evaluation of methodologies to quantify constraint.

2. Application of the two parameter fracture mechanics (J-Q) methodology to quantify the role of constraint on cleavage fracture toughness appeared effective in predicting the fracture behavior of the structurally relevant surface cracked plate geometry.

3. The data range for SC(B) geometry 2 approximates that of the SE(B) specimen with $a/W \approx 0.1$ and the data range for SC(B) geometry 3 approximates that for the SE(B) specimen with $a/W \approx 0.3$. This result implies that toughness scaling constraint analysis of the SC(B) geometries may be possible by estimating the toughness scaling driving force curves for the two SC(B) geometries from the appropriate SE(B) curves.

REFERENCES

1. O'Dowd, N. P. and Shih, C. F., "Family of Crack-Tip Fields Characterized by a Triaxiality Parameter: - Part I. Structure of Fields", *Journal of Mechanics and Physics of Solids*, Vol. 39, pp. 989-1015, 1991.

2. O'Dowd, N. P. and Shih, C. F., "Family of Crack-Tip Fields Characterized by a Triaxiality Parameter: - Part II. Fracture Applications", *Journal of Mechanics and Physics of Solids*, Vol. 40, pp. 939-963, 1992.

3. Kirk, M. T., Koppenhoefer, K. C., and Shih, C. F., "Effect of Constraint on Specimen Dimensions Needed to Obtain Structurally Relevant Toughness Measures." *Constraint Effects in Fracture, ASTM STP 1171*, E. M. Hackett, et al., Eds., American Society for Testing and Materials, Philadelphia, pp. 79-103, 1993.

4. Shih, C. F., O'Dowd, N. P., and Kirk, M. T., "A Framework for Quantifying Crack Tip Constraint," *Constraint Effects in Fracture, ASTM STP 1171*, E. M. Hackett, et al., Eds., American Society for Testing and Materials, Philadelphia, pp. 2-20, 1993.

5. Sumpter, J. D. G., and Forbes, A. T., "Constraint Based Analysis of Shallow Cracks in Mild Steel", *Proceedings of TWI/EWI/IS International Conference on Shallow Crack Fracture Mechanics Test and Applications*, Cambridge, UK, 1992.

6. Anderson, T. L. and Dodds, R. H., Jr., "Specimen Size Requirements for Fracture Toughness Testing in the Transition Region", *Journal of Testing and Evaluation*, Vol. 19, No. 2, pp. 123-134, 1991.

7. Dodds, R. H., Jr., Anderson, T. L., and Kirk, M. T., "A Framework to Correlate a/W Effects on Elastic-Plastic Fracture Toughness (J_c)", *International Journal of Fracture*, Vol. 48, pp. 1-22, 1991.

8. Kirk, M. T., and Dodds, R.H., Jr., "Approximate Techniques of J Estimation Applicable to Part-Through Surface Cracks", *Engineering Fracture Mechanics*, Vol. 43, No. 1, pp. 123-136, 1992.

9. Dodds, R.H., Jr., Shih, C. F., and Anderson, T.L., "Continuum and Micromechanics Treatment of Constraint in Fracture", NUREG/CR-5971, Nuclear Regulatory Commission, Washington, D.C., 36 pp., 1993.

10. Wallin, K., "Statistical Aspects of Constraint with Emphasis on Testing and Analysis of Laboratory Specimens in the Transition Region", *Constraint Effects in Fracture, ASTM STP 1171*, E. M. Hackett, et al., Eds., American Society for Testing and Materials, Philadelphia, pp. 264-288, 1993.

11. Newman, J. C. and Raju, I. S., "Stress-Intensity Factor Equations for Cracks in Three-Dimensional Finite Bodies Subjected to Tension and Bending Loads", NASA Technical Memorandum 85793, NASA Langley Research Center, Hampton, VA, 38 pp., 1984.

12. Turner, C. E., "Further Developments of a J-Based Design Curve and Its Relationship to Other Procedures", *Elastic Plastic Fracture: Second Symposium, Volume II--Fracture Resistance Curves and Engineering Applications, ASTM STP 803*, C. F. Shih and J. P. Gudas, Eds., American Society for Testing and Materials, pp. II-80--II-102, 1983.

13. Ainsworth, R. A., "The Assessment of Defects in Structures of Strain Hardening Material", *Engineering Fracture Mechanics*, Vol. 19, No. 4, pp. 633-642, 1984.

14. Miller, A. G., "Review of Limit Loads of Structures Containing Defects", *International Journal of Pressure Vessels and Piping*, Vol. 32, pp. 197-327, 1988.

15. Joyce, J. A. and Link, R. E., "Effects of Constraint on Upper Shelf Fracture Toughness", *Fracture Mechanics: 26th Volume, ASTM STP 1256*, Walter G. Reuter, John H. Underwood, and James C. Newman, Jr. Eds., American Society for Testing and Materials, Philadelphia, 35 pp., 1995.

INITIAL DISTRIBUTION

OUTSIDE CENTER

Copies		Copies	
6	NAVSEA 1 03M2 1 03P2 1 03P2 (Martino) 1 03P4 1 03P4 (Manuel) 1 08S	1	Brown Univ. 1 (Dr. C. F. Shih)
2	NRL 1 6380 1 6384	1	Univ. of Illinois 1 (Dr. R. H. Dodds)
3	ONR 1 1132 (Rajapakse) 1 1132 (Vasudivan) 1 Lib	1	Texas A&M Univ. 1 (Dr. T. L. Anderson)
1	USNA 1 (Dr. J. Joyce)	2	NASA/Langley 1 Lib 1 (Dr. J. Newman)
2	DTIC		
4	USNRC 1 (M. Mayfield) 1 (Dr. S. Malik) 1 (A. Hiser) 1 (Dr. E. Hackett)		
1	DOE, Oak Ridge		
2	NIST, Boulder 1 Lib 1 (J. Berger)		
4	NIST, Washington, D.C. 1 Lib 1 (R. Fields) 1 (R. DeWitt) 1 (J. T. Fong)		

CENTER DISTRIBUTON

Copies

Copies	
1	0114
1	0115
1	60
1	601
1	602
1	603
1	61
1	61s
1	612
1	613
2	614
5	614 (Link)
10	614 (Porr)
1	615
1	62
1	624
1	625
1	65
1	65.3
1	65.3 (Sickles)
1	65.3 (Gifford)
1	65.3 (Rasmussen)
1	66
1	66.3
1	68
1	68.3
1	3421
1	3422

REPORT DOCUMENTATION PAGE

Form Approved
OMB No. 0704-0188

1. AGENCY USE ONLY (Leave blank)	2. REPORT DATE	3. REPORT TYPE AND DATES COVERED
	AUGUST 1994	RESEARCH AND DEVELOPMENT

4. TITLE AND SUBTITLE
Experimental Application of Methodologies to Quantify the Effect of Constraint on Jc for a 3-D Flaw Geometry

5. FUNDING NUMBERS
Program Element No. 62234N

6. AUTHOR(S)
W. C. Porr, Jr., R. E. Link, J. P. Waskey, and R. H. Dodds, Jr.

7. PERFORMING ORGANIZATION NAME(S) AND ADDRESS(ES)
Naval Surface Warfare Center
Carderock Division
Bethesda, MD 20084-5000

8. PERFORMING ORGANIZATION REPORT NUMBER
CARDIVNSWC/TR-61-94/25

9. SPONSORING /MONITORING AGENCY NAME(S) AND ADDRESS(ES)
Naval Surface Warfare Center
Carderock Division
Code 0115
Bethesda, MD 20084-5000

10. SPONSORING /MONITORING AGENCY REPORT NUMBER

11. SUPPLEMENTARY NOTES

12a. DISTRIBUTION /AVAILABILITY STATEMENT
Approved for public release; distribution is unlimited.

12b. DISTRIBUTION CODE

13. ABSTRACT *(Maximum 200 words)*

In an effort to validate methodoligies to quantify the effect of crack tip constraint on cleavage fracture toughness, a series of experiments were conducted to measure the cleavage fracture toughness, Jc, of an ASTM A515 Grade 70 steel utilizing large plate bend specimens containing semi-elliptical surface cracks, SC(B), (3-D flaw geometry). Jc was estimated with modified EPRI and Turner design curve schemes from load and remote strains measured at initiation. The cleavage toughhess of the A515 steel used for this testing was previously characterized using a series of through-cracked single edge notch bend specimens, SE(B), (2-D flaw geometry) with various initial cracl-length to specimen-width ratios, a/W. The toughness values measured for the surface cracked plate specimens were consistent with the toughness ranges predicted from the SE(B) results using the toughness scaling and two parameter fracture mechanics (J-Q) methodologies to account for differences in crack tip constraint. This result verifies the applicability of small specimen, constraint adjusted, results to engineering structural integrity prediction for the case of cleavage fracture.

14. SUBJECT TERMS	15. NUMBER OF PAGES
Fracture Mechanics, Cleavage, Constraint, Steel, Surface crack, Fracture toughness, J-Integral	19
	16. PRICE CODE

17. SECURITY CLASSIFICATION OF REPORT	18. SECURITY CLASSIFICATION OF THIS PAGE	19. SECURITY CLASSIFICATION OF ABSTRACT	20. LIMITATION OF ABSTRACT
UNCLASSIFIED	UNCLASSIFIED	UNCLASSIFIED	UNCLASSIFIED